

基于无序纳米颗粒的光子晶体有机薄膜

付宸锐¹, 祝明², 刘东旭^{2*}, 赵达²¹北京航空航天大学航空科学与工程学院, 北京 100191;²北京航空航天大学无人系统研究院, 北京 100191

摘要 无序光子晶体有机薄膜的制备是实现光阻隔材料量产的关键。设计了无序多级光子晶体结构有机薄膜,以热塑性聚氨酯作为膜材基质,将二氧化钛颗粒作为反射隔光材料填入基质中。采用时域有限差分法进行了模拟,结果表明,增加填充因子导致了反射峰和光谱禁带的蓝移,而增加颗粒直径造成了光谱禁带红移。将单一直径均匀分布的阵列作为对比,分析了粒径多级性和结构聚结性对光谱的影响。对于横电波和横磁波,在 $0^{\circ}\sim 70^{\circ}$ 的宽入射角范围内实现了高效禁带效应。这种无序光子晶体结构的有机薄膜为宽角度光阻隔材料提供了参考。

关键词 薄膜; 无序光子晶体; 有机薄膜; 光阻隔材料; 二氧化钛颗粒; 时域有限差分法

中图分类号 O436

文献标志码 A

DOI: 10.3788/AOS221934

1 引言

光子晶体被认为是光子的半导体,可以有效调控光子(电磁波)运动方式,禁止或允许某一方向、某些频率光的传输^[1-2]。然而,制备周期性高精度的光子晶体依赖于微纳加工技术如激光光刻、电子束蒸发、高频溅射等^[3-5],这极大限制了光子晶体在低成本批量生产行业中的应用。

无序光子晶体的设计无需高精度的纳米材料和结构^[6-7],其随机排布的电介质和纳米结构同样会产生强烈的 Anderson 局域化效应,光在其中发生布拉格散射,进而产生光子禁带。禁带宽度与结构对称性和介电常数比值有关,结构对称性越差,能带简并度就越低,难以出现光子禁带;而介电常数比值越高,光子禁带则更为明显。无论光的偏振形式和传播方向如何,处于禁带范围内都无法传播。近年来,无序光子晶体的研究极大促进了激光器、谐振器、光纤、太阳能电池光收集器和非侵入式成像系统等领域的发展^[8-9]。

基于这些原理,先前工作中制备了基于无序纳米颗粒的光子晶体有机薄膜,实现了光阻隔应用与日间冷却性能^[10]。仅采用双螺杆造粒和流延成膜技术便可制备理想的无序光子晶体,这种卷对卷可拓展的薄膜可广泛应用于航空航天、汽车、建筑和服装等领域^[11-12]。然而,无序光子晶体的设计参数仍需优化,通过光学仿真研究纳米颗粒的填充因子、粒径分布和结构对称性对光阻隔性能的影响^[13-14],目前国内外研究

主要使用米氏散射理论和蒙特卡罗射线追踪等方法^[15-16],未对薄膜微观结构在时域有限差分域中建模,未对有机聚合物薄膜的离散纳米粒子体系进行设计,缺乏对光在微观结构中传输特性的分析。

本工作研究了设计参数对无序纳米颗粒有机薄膜阻隔特性的影响,增强了光在无序光子晶体中的禁带效应。基于纳米颗粒的粒径分布和介电常数等参数,利用时域有限差分(FDTD)法研究了光在无序阵列中的传输特性,计算了光谱曲线。本文研究了离散分布单一粒径的纳米颗粒的设计参数,考虑了多级粒径尺寸和聚结结构的不对称性影响。研究表明,尽管光子晶体阵列具有随机性和无序性,但通过调整纳米颗粒的填充因子和粒径分布,仍可以显著增强光禁带效应。

2 模型与计算方法

制备了二氧化钛(TiO_2)颗粒的有机薄膜样品,并根据扫描电子显微镜(SEM)图片进行FDTD域建模。首先根据纳米颗粒的填充因子等效计算质量分数 M_f ,在温度为 170°C 和转速为 200 r/min 的搅拌条件下将 TiO_2 纳米颗粒与热塑性聚氨酯TPU母粒充分混合。然后使用双螺杆将混合物挤出设备并造粒,并在 120°C 真空箱中干燥 12 h 。最后使用单螺杆流延机制备离散纳米颗粒的有机薄膜。将薄膜样品放置在SEM下对微观结构进行观察,同一薄膜样品两典型区域的无序光子晶体结构分别如图1(a)和(c)所示, TiO_2 纳米颗粒在聚合物基质中随机分布,对应的简化模型如图1(b)和

收稿日期: 2022-11-04; 修回日期: 2022-12-14; 录用日期: 2023-01-09; 网络首发日期: 2023-01-19

基金项目: 国家自然科学基金(61827901)、中央高校基本科研业务费专项资金(YWF-22-JC-01, YWF-22-JC-02)

通信作者: *liubuaa@163.com

(d)所示。如图 1(a)所示,该区域在优良成膜条件下不具有任何优先成核位置,未发生聚结情况。然而,如

图 1(c)所示,该区域母粒的不均匀性导致颗粒发生聚结,从而生成了高密度大直径的颗粒基团。

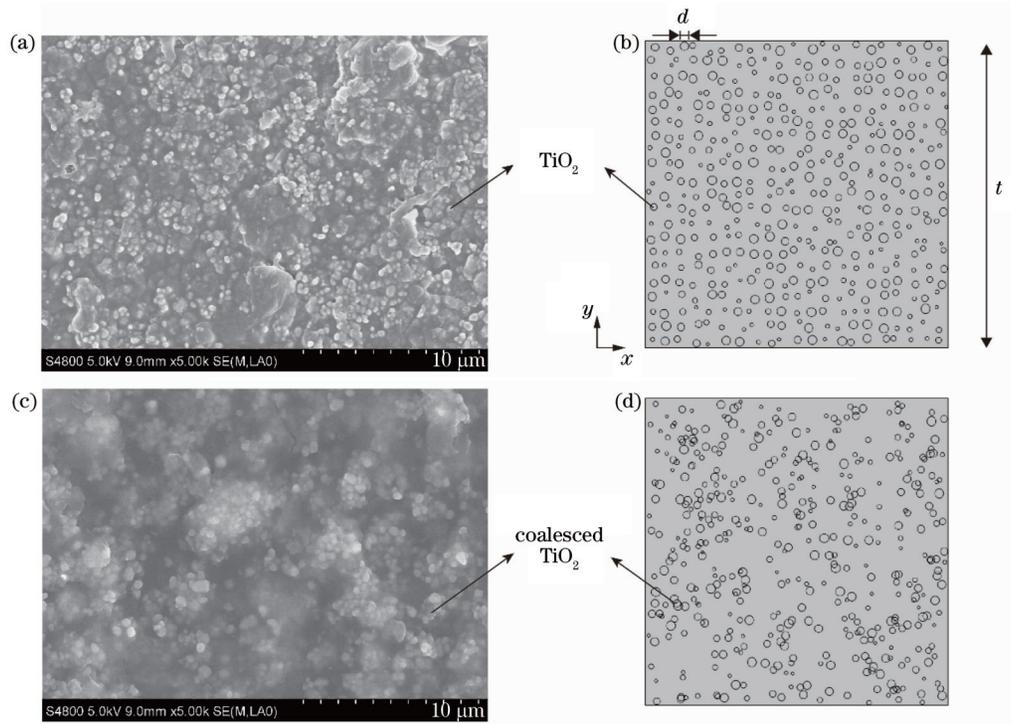


图 1 SEM 图片和纳米颗粒微观模型。(a)纳米颗粒未聚结的薄膜横截面;(b)纳米颗粒未聚结的简化模型;(c)纳米颗粒发生聚结的薄膜横截面;(d)纳米颗粒发生聚结的简化模型

Fig. 1 SEM images and nanoparticle microscopic models. (a) Film cross-section of nanoparticles without agglomeration; (b) simplified model of nanoparticles without agglomeration; (c) film cross-section of nanoparticles with agglomeration; (d) simplified model of nanoparticles with agglomeration

通过时域有限差分法进行电磁场计算,使用 MEEP 软件对薄膜厚度方向的微观电场空间分布和宏观光学特性曲线进行了分析,研究不同设计参数对光传输特性的影响。根据图 1(a)和(c)中 SEM 图像,将该微观结构简化为非偏振平面内的 2D 无序光子晶体,将纳米颗粒近似为圆形。仿真区域高度 t 远大于纳米颗粒的直径 d , 其中 d 和填充因子 M_f 根据实际进行设置。在大多数研究中^[12, 16], 制备样品采用的实际 TiO_2 纳米颗粒直径 d 通

常为 100 nm 至 1 μm 。如图 2(a)所示,使用激光粒度仪 Mastersizer-2000 对本实验中 TiO_2 颗粒进行了粒径分布测试,有约 63.6% 的颗粒直径分布在 10~210 nm, 而 36.4% 的颗粒直径分布在 276~1875 nm。该结果与 SEM 图片基本一致,由此表明,制成样品后颗粒尺度未发生明显变化。如图 2(b)和(c)所示,根据先前文献设置了 TiO_2 颗粒^[17] 和有机聚合物基质^[18] 的光学参数,其中 n 和 k 分别为折射率和消光系数。

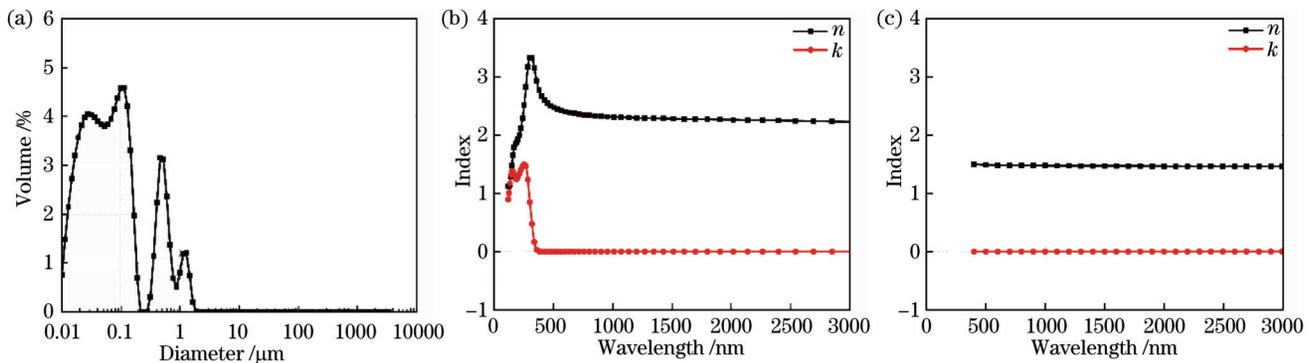


图 2 材料的粒径分布和光学参数曲线。(a) TiO_2 的粒径分布;(b) TiO_2 的折射率和消光系数;(c) TPU 的折射率和消光系数

Fig. 2 Particle size distribution and optical parameter profiles of materials. (a) Particle size distribution of TiO_2 ; (b) refractive index and extinction coefficient of TiO_2 ; (c) refractive index and extinction coefficient of TPU

3 数值模拟结果和讨论

3.1 填充因子和颗粒直径的影响

为了研究填充因子和颗粒直径变化的影响,根据设计参数对无序纳米颗粒阵列进行了FDTD域建模,其中TiO₂颗粒直径为100~300 nm,填充因子为10%~50%。通过计算电场空间分布和透射率、反射率光谱,评估了各阵列的光子禁带效应。在相同颗粒直径和填充因子条件下,TiO₂颗粒无序分布的随机性会对结果产生影响。因此,对每一种参数设置的阵列都进行8次建模和计算,进而消除了随机性的影响,并对每次透射率、反射率结果进行了平均化处理。

首先研究了TiO₂颗粒的填充因子对薄膜光谱的影

响。保持颗粒直径 $d=100$ nm恒定,创建了填充因子为10%~50%的随机阵列。随着填充因子的增加,在原TPU基质位置中插入新的TiO₂颗粒,进而导致更多次的散射、反射和折射。图3(a)中随着填充因子的增加,1000 nm波长处透射率迅速降低,光谱禁带效应增强。如图3(b)所示,随着填充因子的增加,反射强度增加,反射峰逐渐向短波移动。结果表明:填充因子 $M_f=10\%$ 时,禁带宽度较宽,为200~1500 nm,但是透射率更高;但当 $M_f>45\%$ 时,禁带宽度为较窄的200~1100 nm的波长范围,与低填充因子相比1000 nm处反射率更高。因此,为产生最优光谱禁带效应,TiO₂颗粒的最佳填充因子应在35%~45%之间。值得注意的是,实验室制备成膜的最佳条件也在此范围。

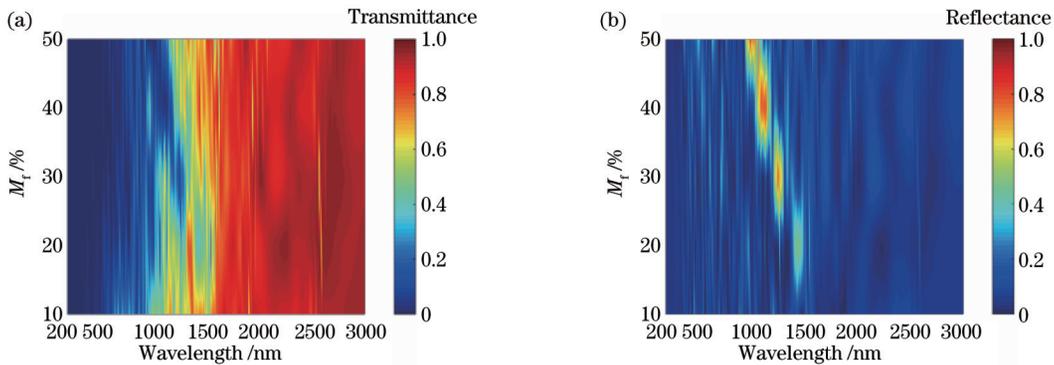


图 3 TiO₂颗粒薄膜光谱随填充因子的变化。(a)透射率;(b)反射率

Fig. 3 Variations of TiO₂ particle film spectra with filling factor. (a) Transmittance; (b) reflectance

进一步研究了填充因子为40%时,薄膜中纳米颗粒直径分别为100 nm、200 nm、300 nm的光谱。如图4(a)所示,以上三种粒径分别在200~1000 nm、200~1500 nm和200~2500 nm的波长范围内获得了低透射

率值,这些低透射率区间对应于光子禁带效应。结果表明,随着纳米颗粒直径的增加,图4(a)中禁带区域向长波波段移动,图4(b)中反射峰也出现了红移现象,这与图3(a)中填充因子增加时观察到的蓝移现象相反。

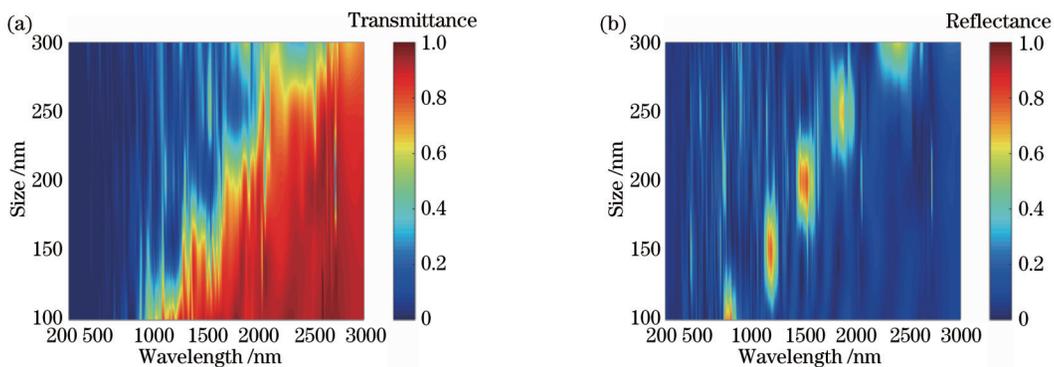


图 4 TiO₂颗粒薄膜光谱随纳米颗粒直径的变化。(a)透射率;(b)反射率

Fig. 4 Variations of TiO₂ particle film spectra with nanoparticle diameter. (a) Transmittance; (b) reflectance

为了进一步研究颗粒直径对电磁波的影响,采用电场空间分布图描述了光波在TiO₂无序光子晶体中的传输特性。图5(a)~(c)分别显示了100~300 nm直径的纳米颗粒阵列在典型波长下的电场空间分布。对于波长为200 nm的光,纳米颗粒直径为100 nm时,空间电场分布局限于阵列的上部区域,禁带效应区域

光波的电场分量 E_z 为0,表示光在随机阵列中产生强烈的Anderson局域化效应。800 nm的光在三种粒径的阵列中均能传播到薄膜底面,由于发生了多次散射,底面光波相位并不同步。1600 nm波长的电磁波在100 nm颗粒阵列中的传播则不受阻挡,到达底面的光的相位几乎都达到波峰;而200 nm、300 nm颗粒阵列

中到达底面的光则会发生多次散射,导致透射率降低。当光波长为 3000 nm 且远大于纳米颗粒直径时,光在薄膜中的传播无散射效应,电场空间分布将不再受 TiO₂ 颗粒的影响,光的传输特性与在均匀聚合物基质

中一致。因此,随着纳米颗粒直径的增加,光子禁带区域向长波移动,该结论与图 4(a) 中粒径增加导致的禁带区域红移现象一致。

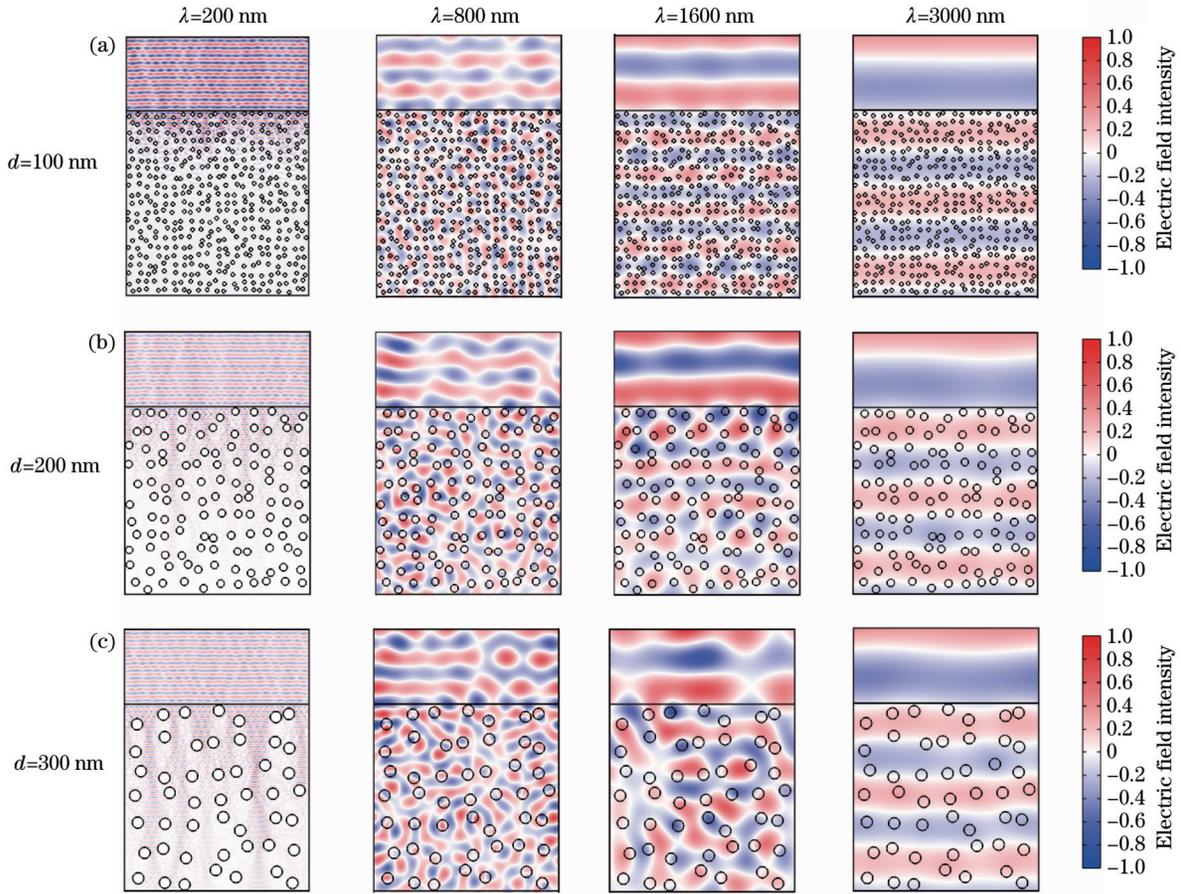


图 5 波长为 200 nm、800 nm、1600 nm 和 3000 nm 的光的电场空间分布。(a) $d=100$ nm; (b) $d=200$ nm; (c) $d=300$ nm
Fig. 5 Spatial distributions of electric field for wavelengths of 200 nm, 800 nm, 1600 nm, and 3000 nm. (a) $d=100$ nm; (b) $d=200$ nm; (c) $d=300$ nm

3.2 粒径多级性和结构聚结性的影响

研究了粒径多级性和结构聚结性对光传输特性的影响。在薄膜制备过程中,由于纳米颗粒直径和有机基质的不均匀性,实际无序光子晶体粒径为多级分布 [图 2(a)], 且在有机基底中易发生聚结现象

[图 1(c)]。

设置填充因子 $M_f=40\%$, 图 6(a)~(c) 描述了 1500 nm 近红外波长的光在三种典型分布中的电场分布。如图 6(a) 所示, 1500 nm 的光在单一颗粒 (直径 $d=100$ nm) 阵列中未发生强烈散射, 薄膜底面电磁波

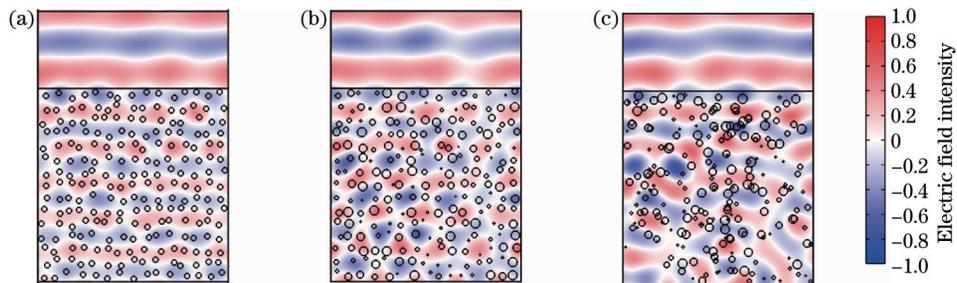


图 6 波长为 1500 nm 的光的空间电场分布。(a) 单一颗粒直径 $d=100$ nm; (b) 多级颗粒直径 $d=(100\pm 50)$ nm; (c) 颗粒结构发生聚结
Fig. 6 Spatial distributions of electric field for light with wavelength of 1500 nm. (a) Single particle diameter $d=100$ nm; (b) hierarchical particle diameter $d=(100\pm 50)$ nm; (c) agglomerated particle structures

的相位几乎都达到波谷,未形成光子带隙;图 6(b)中多级纳米颗粒的直径设置为 (100 ± 50) nm,电磁波发生了多次散射,导致透射率降低,薄膜底面部分电磁波波峰与波谷同时出现。图 6(c)中多级纳米颗粒产生聚结现象,颗粒基团无序度增加导致散射程度进一步提高,证明该结构对 1500 nm 波长的光仍会形成光子带隙。

三种典型分布的透射率光谱和实验结果的对比如图 7(a)和(b)所示。分析结果表明:在 1500 nm 波长处,单一粒径均匀分布的阵列的透射率为 62%,多级粒径阵列的透射率为 30%,多级性和聚结性同时存在

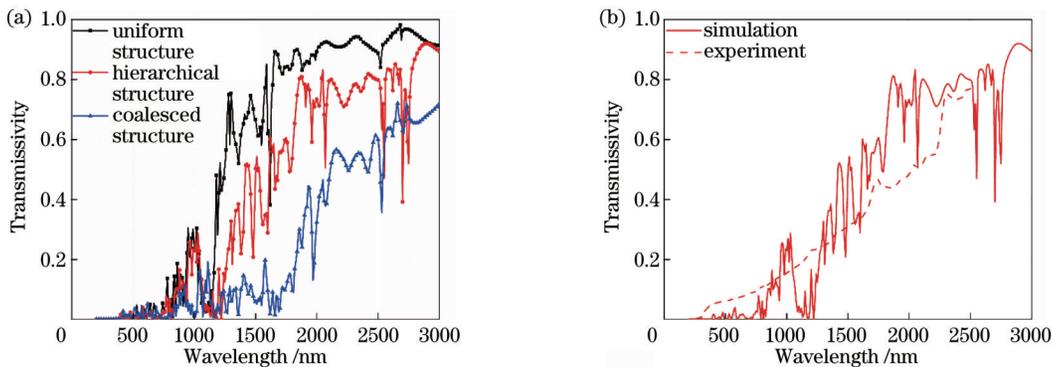


图 7 透射率曲线。(a)三种结构透射率对比;(b)仿真结果与实验结果对比

Fig. 7 Transmittance curves. (a) Comparison of transmittance of three structures; (b) comparison of simulation results with experimental results

3.3 宽角度光阻隔能力

为评估薄膜的广角光阻隔能力,本节通过仿真对薄膜在 TE 和 TM 偏振波下的透射率曲线进行了分析。设置颗粒直径 $d=(100 \pm 50)$ nm 的聚结结构,填充因子 $M_f=40\%$,入射角度 θ 为 $0^\circ \sim 80^\circ$ 。图 8(a)、(b)

时透射率则会降低至 8%。这些值与图 6(a)~(c)中讨论的结果一致。为验证结果的正确性,使用紫外可见光近红外分光光度计 UV3600 测量了薄膜样品在 200~2500 nm 波长范围内的透射率光谱。与图 7(b)中实验测得的光谱透射率相比,多级粒径阵列的仿真结果有良好的一致性。但是,在 1500~2200 nm 近红外波段,实际透射率比仿真结果低 20%。这是因为薄膜样品在某些微观区域发生了图 1(c)、图 6(c)所示的聚结现象,进而在 1500~2200 nm 处形成了光子带隙。因此,纳米颗粒的多级性和聚结性对有机薄膜的近红外波段透射率产生了重大影响。

模拟了透射率曲线随入射角的变化,薄膜在 $0^\circ \sim 70^\circ$ 的宽入射角范围内实现了对 200~600 nm 波长的高效禁带效应,但是对 600~3000 nm 波长光的阻隔能力在一定程度上受到限制。其中入射角 $\theta=0^\circ$ 时,TE 模透射率仿真结果与图 7(b)中实验测量结果一致。

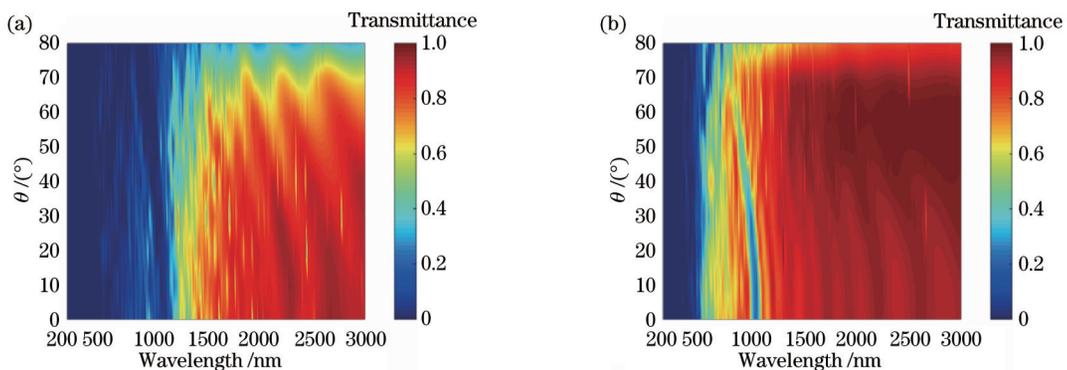


图 8 透射率曲线随入射角 θ 的变化。(a) TE 模;(b) TM 模

Fig. 8 Variation of transmittance with angle of incidence θ . (a) TE mode; (b) TM mode

图 9(a)与(b)分析了 TE 模电磁波的电场空间分布。对于波长 $\lambda=300$ nm 的光,在宽入射角范围内都只传播到薄膜浅层,无法传播至底面。而对于波长 $\lambda=2000$ nm 远超粒径的电磁波, TiO_2 颗粒对不同入射角度的光均难以发挥阻隔作用。由此可见,本文设计的无序光子晶体在可见光与近红外范围内具有良好的

广角光阻隔能力。

4 结 论

设计并制备了无序光子晶体有机薄膜,研究了设计参数对薄膜光子禁带效应的影响。随着填充因子 M_f 的增加,反射峰和光谱禁带均向短波移动,但是反

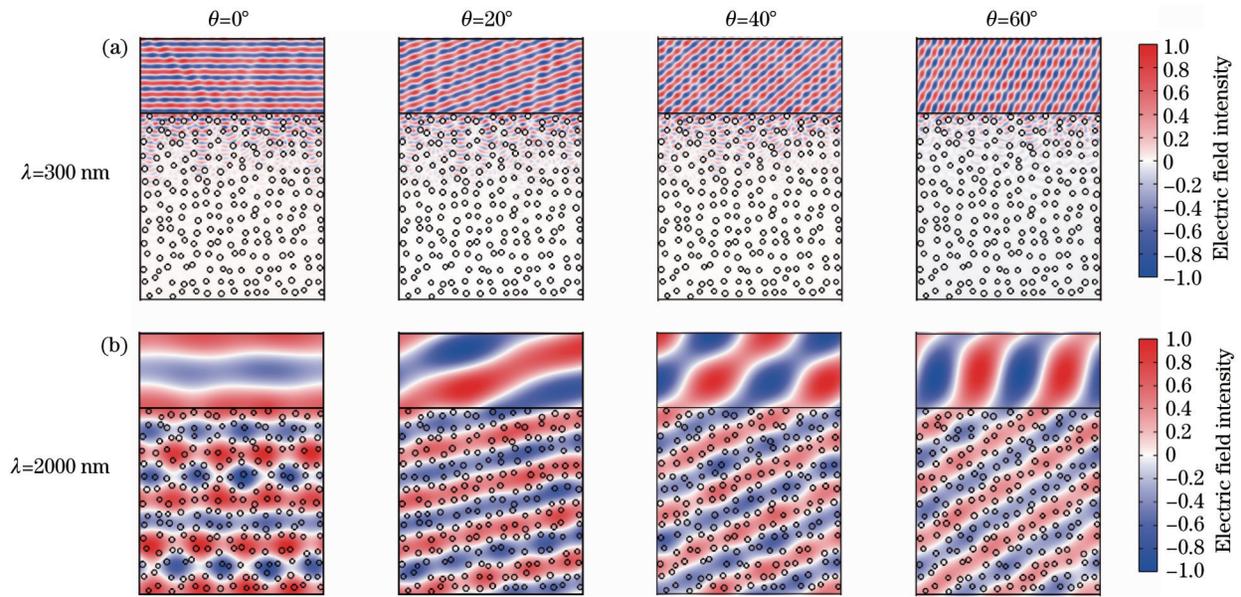


图 9 入射角 θ 为 0° 、 20° 、 40° 和 60° 的电场空间分布。(a) 波长为 300 nm; (b) 波长为 2000 nm

Fig. 9 Spatial distributions of electric fields with incidence angles θ of 0° , 20° , 40° , and 60° . (a) Wavelength of 300 nm; (b) wavelength of 2000 nm

射峰强度增加。为产生最优光谱禁带效应, TiO_2 颗粒的最佳填充因子应在 $35\% \sim 45\%$ 之间。 TiO_2 纳米颗粒直径增加导致禁带区域红移现象, 增强了近红外光的散射和阻隔能力。与单一直径均匀分布的阵列相比, 粒径多级性和颗粒聚结性使近红外光透射率降低了 54% 。TE 模和 TM 模偏振光在 $0^\circ \sim 70^\circ$ 的宽入射角范围内实现了对 $200 \sim 600$ nm 波长的高效禁带特性。本研究对无序光子晶体的参数进行了优化设计, 尤其是对 TiO_2 纳米颗粒有机薄膜的制备提供了理论支持。

参 考 文 献

- [1] Yablonovitch E. Inhibited spontaneous emission in solid-state physics and electronics[J]. Physical Review Letters, 1987, 58(20): 2059-2062.
- [2] John S. Strong localization of photons in certain disordered dielectric superlattices[J]. Physical Review Letters, 1987, 58(23): 2486-2489.
- [3] 梁文耀, 杨佳琪, 李志远. 多光束全息干涉法制作复式光子晶体的数值仿真研究[J]. 光学学报, 2021, 41(11): 1116002. Liang W Y, Yang J Q, Li Z Y. Numerical simulation on fabricating compound photonic crystals by multi-beam holographic interferometry[J]. Acta Optica Sinica, 2021, 41(11): 1116002.
- [4] 潘智鹏, 李伟, 戚宇轩, 等. 光子晶体垂直腔面发射激光器的设计分析[J]. 光学学报, 2022, 42(14): 1414002. Pan Z P, Li W, Qi Y X, et al. Design and analysis of photonic crystal vertical-cavity surface-emitting lasers[J]. Acta Optica Sinica, 2022, 42(14): 1414002.
- [5] 孙大伟, 李长红, 易凌俊, 等. 基于二维光子晶体的宽带高吸收太阳能吸收器[J]. 光学学报, 2021, 41(5): 0516002. Sun D W, Li C H, Yi L J, et al. High absorption broadband solar energy absorber based on two-dimensional photonic crystal [J]. Acta Optica Sinica, 2021, 41(5): 0516002.
- [6] Wiersma D S. Disordered photonics[J]. Nature Photonics, 2013, 7(3): 188-196.
- [7] 陈剑锋, 梁文耀, 李志远. 磁光光子晶体中拓扑光子态研究进展[J]. 光学学报, 2021, 41(8): 0823015. Chen J F, Liang W Y, Li Z Y. Progress of topological photonic state in magneto-optical photonic crystal[J]. Acta Optica Sinica, 2021, 41(8): 0823015.
- [8] Cao H. Review on latest developments in random lasers with coherent feedback[J]. Journal of Physics A: Mathematical and General, 2005, 38(49): 10497-10535.
- [9] Lagendijk A, Tiggelen B V, Wiersma D S. Fifty years of Anderson localization[J]. Physics Today, 2009, 62(8): 24-29.
- [10] Fu C R, Zhu M, Zhao D, et al. Daytime radiative cooling capacity of nanoparticle on thermoplastic polyurethane (TPU) film[J]. Solar Energy, 2022, 245: 322-331.
- [11] Li W X, Li Y R, Shah K W. A materials perspective on radiative cooling structures for buildings[J]. Solar Energy, 2020, 207: 247-269.
- [12] Zeng S N, Pian S J, Su M Y, et al. Hierarchical-morphology metafabric for scalable passive daytime radiative cooling[J]. Science, 2021, 373(6555): 692-696.
- [13] Paul D J, Mimi A A, Hazari A, et al. Finite-difference time-domain analysis of the tunability of Anderson localization of light in self-organized GaN nanowire arrays[J]. Journal of Applied Physics, 2019, 125(4): 043104.
- [14] 温清凌, 谢应茂. 部分无序二维光子晶体透射特性研究[J]. 激光杂志, 2010, 31(1): 34-35. Wen Q L, Xie Y M. The optical transmission characteristics in two dimension photonic crystal with part disorder[J]. Laser Journal, 2010, 31(1): 34-35.
- [15] Cheng Z M, Wang F Q, Wang H, et al. Effect of embedded polydisperse glass microspheres on radiative cooling of a coating [J]. International Journal of Thermal Sciences, 2019, 140: 358-367.
- [16] Peoples J, Li X Y, Lü Y B, et al. A strategy of hierarchical particle sizes in nanoparticle composite for enhancing solar reflection[J]. International Journal of Heat and Mass Transfer, 2019, 131: 487-494.
- [17] Siefke T, Kroker S, Pfeiffer K, et al. Materials pushing the application limits of wire grid polarizers further into the deep ultraviolet spectral range[J]. Advanced Optical Materials, 2016, 4(11): 1780-1786.
- [18] Zhang X N, Qiu J, Li X C, et al. Complex refractive indices

Organic Films with Photonic Crystals Based on Disordered Nanoparticles

Fu Chenrui¹, Zhu Ming², Liu Dongxu^{2*}, Zhao Da²

¹*School of Aeronautic Science and Engineering, Beihang University, Beijing 100191, China;*

²*Institute of Unmanned System, Beihang University, Beijing 100191, China*

Abstract

Objective The random arrangement of dielectrics and nanostructures in disordered photonic crystals produces strong Anderson localization effect and does not require high-precision nanomaterials and structures. In the previous study, we reported photonic crystal organic films with disordered nanoparticles, which were a roll-to-roll expandable material for various applications in aerospace, automotive, construction, and apparel. However, the design parameters of disordered photonic crystals still need to be optimized. This paper aims to investigate the effect of fill factor, particle size distribution, and structural symmetry of nanoparticles on the light-insulation properties by using a finite-difference time-domain (FDTD) method. The discrete nanoparticle system of organic polymer films should be further designed by analyzing the light transport properties in the microstructure.

Methods Organic film samples of discrete nanoparticles are prepared by using the tape casting method. The microstructure of TiO₂ particles is observed by scanning electron microscopy and modeled in the FDTD. The nanostructure is simplified to a two-dimensional (2D) disordered photonic crystal in the non-polarized plane, with the particle size and the fill factor set according to experimental measurements. Electromagnetic field calculation is carried out by the FDTD method to analyze the microscopic electric field spatial distribution and macroscopic optical characteristic curves. Then the effect of different design parameters on the optical transmission characteristics is investigated. On the basis of SEM photographs, models of hierarchical size and agglomerated structures are established, and the electric field distribution of light waves in three typical structures is calculated and compared with the experimental transmittance curves. Floquet periodicity boundary conditions are set to investigate the propagation characteristics of polarized lights at different incident angles, and the wide-angle light-blocking capability is verified.

Results and Discussions The effects of the fill factor and particle diameter of TiO₂ particles on the film spectra are investigated, and the spatial distribution of the electric field is used to describe the transmission characteristics of light waves in disordered TiO₂ photonic crystals. At a fill factor of $M_f=10\%$, the forbidden band width is wider in the range of 200–1500 nm, and the transmittance is higher. However, when M_f is larger than 45%, the forbidden band width is narrower in the wavelength range of 200–1100 nm, and the reflectance is higher at 1000 nm compared with that at a low fill factor. The results suggest that the optimal fill factor for TiO₂ particles shall fall in the range of 35%–45%, so as to produce the best spectral forbidden band effect. As the nanoparticle diameter increases, the forbidden band region shifts towards the long wavelength band, and the reflection peaks become redshifted, in contrast to the blue shift observed when the fill factor increases. For a wavelength of 200 nm, the spatial electric field distribution is confined to the upper region of the array for nanoparticle diameter of 100 nm. The light of 800 nm propagates to the bottom surface of the film in the array with three particle sizes, but the phases are not synchronous. For electromagnetic waves with a length of 1600 nm, their propagation is unobstructed in the array of 100 nm, and the phase of the light reaching the bottom surface almost always reaches the wave peak, while the light reaching the bottom surface in the arrays of 200 nm and 300 nm undergoes multiple scattering and results in reduced transmittance. When the light wavelength is 3000 nm, much larger than the nanoparticle diameter, the light propagates through the film without scattering effects, the spatial distribution of the electric field is no longer influenced by the TiO₂ particles, and the light transmission properties are consistent with those in a homogeneous polymer matrix. The effects of hierarchical particle size and structural aggregation on the light transmission properties are further investigated and compared with experimental results, which result in a 54% reduction in near-infrared (NIR) light transmission. Finally, the wide-angle light-blocking capability of the films is evaluated. Then the transmittance profiles and electric field spatial distribution at polarized waves are analyzed. For TE- and TM-mode polarized light, efficient band-blocking properties are achieved over a wide incidence angle range of 0°–70° for wavelengths of 200–600 nm. For a wavelength of 300 nm similar to the particle size, the light propagates only to the shallow layers of the film over a wide range of incidence angles. For a wavelength of 2000 nm, which is well beyond the particle size, TiO₂ particles have

difficulty in blocking light. This study provides theoretical support for the optimal design of parameters for disordered photonic crystals, especially for the preparation of organic films of TiO_2 nanoparticles.

Conclusions The preparation of disordered photonic crystal organic films is the key to achieving mass production of light-insulation materials. In this paper, hierarchically disordered photonic crystal structured organic films are designed by using thermoplastic polyurethane as the film substrate and titanium dioxide particles as the reflective barrier material filling the substrate. Simulations are carried out by using the FDTD method, and the results show that the increase in fill factor causes a blue shift in the reflection peak and spectral forbidden band, while the increase in particle diameter causes a red shift in the spectral forbidden band. Compared with arrays with a uniform distribution and a single diameter, the effects of hierarchical particle size and structural aggregation on NIR waves are analyzed. For both transverse electric and transverse magnetic waves, efficient forbidden band effects are achieved over a wide incidence angle range of 0° – 70° . Such organic films containing disordered photonic crystal structures provide a reference for wide-angle light-insulation materials.

Key words thin films; disordered photonic crystal; organic film; light-insulation materials; titanium dioxide particles; finite-difference time-domain method